Low Temperature Synthesis of Nanocrystallized Titanium Oxides with Layered or Tridimensional Frameworks, from $[Ti_8O_{12}(H_2O)_{24}]Cl_8 \cdot HCl \cdot 7H_2O$ Hydrolysis

Chia-Erh Liu,[†] Annabelle Rouet,[†] Hari Sutrisno,[†,‡] Eric Puzenat,[†,§] Hélène Terrisse,[†] Luc Brohan,*[,†] and Mireille Richard-Plouet*[,†]

Institut des Matériaux Jean Rouxel, Université de Nantes, CNRS 2, rue de la Houssinière BP32229, 44322 NANTES Cedex, France, Department of Chemistry, Faculty of Mathematic and Natural Sciences, Yogyakarta State University, Karangmalang, 55281 Yogyakarta, Indonesia, and IRCELYON Institut de recherches sur la catalyse et l'environnement de Lyon, UMR 5256 CNRS-Université Lyon, 2 Avenue Albert Einstein, 69629 Villeurbanne Cedex, France

Received March 11, 2008. Revised Manuscript Received May 5, 2008

A low-temperature aqueous chemical growth process was developed to produce nanometric titanium oxide with controlled size and structural variety. Gentle hydrolysis of a commercial $TiOCl_2$ solution, in a controlled relative humidity, leads to the formation of single crystals of $[Ti_8O_{12}(H_2O)_{24}]Cl_8 \cdot HCl \cdot 7H_2O$. Under autogenous pressure at 120 °C, the hydrolysis of the latter by tetramethylammonium hydroxide (noted TMAOH) is mainly governed by the R = Ti/TMAOH molar ratio and thus by the pH value. Two values are particularly important: R = 8/9 and 8/17. The former corresponds to the balance of the Cl^- ions of the titanium oxychloride hydrate by TMA^+ cations and the latter to the stoichiometric ratio for the formation of a layered oxo-hydroxide $(TMA)_2Ti_2O_{4-x}(CO_3)_x(OH)_2 \cdot nH_2O$, $x = 0.7$, which is obtained under basic conditions. Above R = 8/9, that is, in an acidic medium, the solvothermal treatment at 120 °C directly leads to the crystallization of anatase and then rutile when the pH decreases. For intermediate R values, the amorphous dried solid is required to be rinsed and dried at 110 °C to lead to the crystallization of nanometric titania, either anatase or brookite. TEM studies show that titania nanoparticles exhibit superstructures involving a doubling of the cell parameters that could originate from the adsorption of carbonate, hydrogen carbonate, or hydroxyl groups on the nanocrystallite surface. During evaporation of the solvent, these crystallites can self-assemble to form micrometric platelets.

Introduction

Among the technologies making use of the properties of titanium oxide, the photoactivity of TiO_2 is certainly one of the most attractive properties. The creation of an electron-hole pair under UV irradiation on TiO_2 and the chemical or electron transfer reactions which follow are at the heart of the development of photodevices. Furthermore, in addition to the particular applications connected to the exploitation of this property, such as oxidation photocatalysis of organic molecules, water splitting, and superhydrophilicity, titanium dioxide also finds applications in photovoltaic devices. The dye-sensitized solar cells (DSSC)[1] consist of a nanostructured film of titanium dioxide (TiO_2) coated on a substrate of conductive glass. In such devices, the crucial role of the TiO_2 layer deposited on the transparent conductive electrode has been demonstrated.[2] The layer is required on the one hand to be dense to avoid any short circuits between the electrolyte and the electrode and on the other hand to be nanostructured to enhance the collection of charge carriers. In this particular application, a thin dense titania layer has thus been optimized. Several methods have been reported including spray pyrolysis,[3] electrodeposition,[2a] dip coating,[4] and evaporation induced self-assembly leading to a mesoporous titania film.[5] Generally, crystallizing titania requires thermal treatment at high temperature (T > 450 °C). This may be a severe drawback regarding adhesion of the film on the substrate and may also destroy the initial self-organization.

Among the different syntheses, the use tetramethyl- or tetrabutylammonium hydroxide to promote hydrolysis and condensation of Ti alkoxides leads to remarkable results regarding the control of the morphology of titania. In particular, Chemseddine and Moritz have reported that anatase can be grown either as nanorods or spheres using TMAOH to hydrolyze Ti isopropoxide under reflux to

* Corresponding authors. M.R.-P.: e-mail mireille.richard@cnrs-imn.fr, tel +33 240 37 39 96, fax +33 240 37 39 95. L.B.: e-mail luc.brohan@cnrs-imn.fr, tel +33 240 37 39 35, fax +33 240 37 39 95.

[†] Université de Nantes CNRS.

[‡] Yogyakarta State University.

[§] UMR 5256 CNRS-Université Lyon.

(1) O'Regan, B.; Grätzel, M. *Nature* **1991**, *353*, 737.

(2) (a) Gregg, B. A.; Pichot, F.; Ferrere, S.; Fields, C. L. *J. Phys. Chem. B* **2001**, *105*, 1422. (b) Nogueira, A. F.; Longo, C.; De Paoli, M. A. *Coord. Chem. Rev.* **2004**, *248*, 1455. (c) Spiekermann, S.; Smestad, G.; Kowalik, J. L.; Tolbert, M.; Grätzel, M. *Synth. Met.* **2001**, *121*, 1603.

(3) Krüger, J.; Plass, R.; Piccirelli, M.; Grätzel, M.; Bach, U. *Appl. Phys. Lett.* **2001**, *79*, 2085.

(4) Hart, J. N.; Menzies, D.; Cheng, Y. B.; Simon, G.; Spiccia, L. *C. R. Chim.* **2006**, *9*, 622.

(5) (a) Hou, K.; Tian, B.; Li, F.; Bian, Z.; Zhao, D.; Huang, C. *J. Mater. Chem.* **2005**, *15*, 2414. (b) Lancelle-Beltran, E.; Prene, P.; Boscher, C.; Belleville, P.; Buvat, P.; Lambert, S.; Guillet, F.; Boissière, C.; Grosso, D.; Sanchez, C. *Chem. Mater.* **2006**, *18*, 6152.

10.1021/cm800716f CCC: $40.75
Published on Web 06/26/2008

promote crystal nucleation.[6] Other reactants such as titanium oxo-carboxylates were also used to obtain nanocrystalline anatase by autoclaving in presence of TMAOH.[7]

We develop an original acid−base method using a titanium salt as precursor. Instead of the usual reactants for Ti precursors such as titanium alkoxides ($Ti(OC_3H_7)_4$, $Ti(OC_4H_9)_4$) or titanium oxide acetylacetonate ($((CH_3COCH{=}C(O{-})CH_3)_2TiO$), we use a laboratory-made titanium oxychloride hydrate: $[Ti_8O_{12}(H_2O)_{24}]Cl_8 \cdot HCl \cdot 7H_2O$. Its synthesis and characterization will be reported elsewhere. We studied the hydrolysis of this precursor by tetramethylammonium hydroxide (TMAOH) under autogenous conditions at 120 °C. The R = Ti/TMAOH molar ratio was varied from 1/3 to 3/2, that is, from pH range 14 to 0.5 in the supernatant of the suspension, before autoclaving.

Experimental Section

Synthesis. Centimetric crystals of $[Ti_8O_{12}(H_2O)_{24}]Cl_8 \cdot HCl \cdot 7H_2O$ can be obtained in 5 weeks by slow hydrolysis of a commercial $TiOCl_2$ solution (Millenium). This solution is placed in a closed container in which the relative humidity (RH) is maintained between 50 and 60%.[8] Single crystals of this titanium oxychloride hydrate were already isolated from the reaction of $TiCl_4$ with H_2O and were characterized as $[Ti_8O_{12}(H_2O)_{24}]Cl_8 \cdot HCl \cdot 7H_2O$.[9] The powder X-ray diffraction (XRD) pattern of these crystals matches that previously reported for $TiCl(OH)_3 \cdot 2H_2O$.[10]

A total of 8×10^{-4} mol of $[Ti_8O_{12}(H_2O)_{24}]Cl_8 \cdot HCl \cdot 7H_2O$ (1.163 g) and the required amount of $TMAOH \cdot 5H_2O$ are mixed in water (10 mL). Before transferring to the PTFE autoclave, the reactants are stirred for 3 h, at room temperature. For R = Ti/TMAOH ≤ 0.8, the mixture forms a sol, whereas for $0.9 \leq R \leq 1.1$, there is a precipitate which dissolves when R is increased to 1.5. The solvothermal treatment is conducted for 48 h at 120 °C and resulted in a suspension. Drying at 110 °C in air leads to a white and highly hygroscopic powder due to the tetramethylammonium chloride (TMACl) formed in the reaction. Further rinsing with water dissolves the latter, and after drying at 110 °C the powder is no longer hygroscopic. The evolution of titanium oxide during this step has been studied.

Characterization. XRD patterns are collected on an INEL diffractometer, equipped with a curved detector, ranging from 0 to 120°. The powders are set in a Lindeman glass capillary (0.3 mm diameter) which is closed to prevent any interaction with the atmospheric humidity. XRD data were also collected on a Siemens D5000 diffractometer with Cu Kα radiation in Bragg−Brentano geometry. In situ thermal evolution of the XRD patterns were recorded using a Bruker D8 Advance diffractometer, equipped with an Anton Paar HTK 1200N oven chamber. The heating rate was 30 K/min, and after equilibration of the temperature for 5 min, a diffractogramm is recorded, under air, every 50 °C from room temperature to 575 °C.

Transmission electron microscopy (TEM) studies were carried out with a Hitachi H9000NAR electron microscope operating at 300 kV with a Scherzer resolution of 1.8 Å. The solids were ground and dispersed in ethanol prior to being deposited on a copper grid covered with a carbonaceous membrane allowing the observation in TEM. To reduce irradiation damage produced by the electron beam on the sample, the size of the condenser aperture was reduced. Image calculations were performed using the MACTEMPAS program.[11]

Thermogravimetric analysis (TGA/MS) analysis was performed under air at a 1 K/min heating rate, using a SETARAM TG 92, or under Ar when a mass spectrometer is coupled to analyze the gaseous products.

The density measurements were carried out at room temperature by means of an ACCUPYC 1330 Pycnometer (Micromeritics) (high accuracy with a total volume of 1 mL, ΔV is smaller than 0.1 μL).

Infrared spectra were measured using a FTIR Nicolet 20SXC spectrometer in the range 400−4000 cm^{-1}. Powders were ground with dried KBr and then pressed to obtain a pellet (1.3 cm in diameter) suitable for transmission mode.

The X-ray photoelectron spectroscopy (XPS) spectra were recorded on a Kratos Axis Ultra photoelectron spectrometer using a monochromatic Al K source (1486.6 eV) operating at 150 W. The powders were pressed to obtain flat surfaces. As a result of the isolating nature of our samples, charge compensation was accomplished using low-energy electrons flow gun (−2.59 V as bias voltage). High-resolution spectra corresponding to energy regions of interest (O 1s, Ti $2p_{3/2}$, N 1s, and C 1s core level XPS processes) were recorded using a pass energy of 40 eV. The quantification was performed using CasaXPS[12] from the photoelectron peak areas using Shirley background subtraction. Spectra were calibrated in binding energy with C 1s assumed at 284.7 eV for pollution carbon.

Scanning electron microscopy (SEM) images were obtained by using a JEOL 6400F with a tungsten cathode field emission gun operating at 10 kV.

Results and Discussion

The charge balance of Cl^- ions in the titanium oxychloride hydrate, $[Ti_8O_{12}(H_2O)_{24}]Cl_8 \cdot HCl \cdot 7H_2O$, is obtained for R = Ti/TMAOH = 8/9 = 0.89, according to

$$[Ti_8O_{12}(H_2O)_{24}]Cl_8 \cdot HCl \cdot 7H_2O + 9TMAOH \cdot 5H_2O \rightarrow 8(TiO_2 \cdot nH_2O) + 9TMACl + (81 - 8n)H_2O \quad (1)$$

As shown in Figure 1, the intense narrow peaks are attributed to the tetragonal variety of TMACl (JCPDF file no. 21-1922). In addition, depending on the R = Ti/TMAOH ratio, the XRD patterns are characteristic of a bidimensional (2D) framework for R lower than or equal to 0.47 (8/17) and of a tridimensional (3D) arrangement (anatase, anatase and rutile, and then rutile) for $R \geq 0.89$ (8/9). For intermediate R values, the detectable peaks attributed to the 2D phase continuously decrease. Above R = 8/9, the conditions are acid, and the previous equation becomes

(6) Chemseddine, A.; Moritz, T. *Eur. J. Inorg. Chem.* **1999**, 235.
(7) Rammal, A.; Brisach, F.; Henry, M. *C. R. Chim.* **2002**, *5*, 59.
(8) Brohan, L.; Sutrisno, H.; Puzenat, E.; Rouet, A.; Terrisse, H. French CNRS Patent 0305619, May 9, 2003; International Publication WO 2004/101436 A2, Nov 25, 2004; European CNRS patent (EP) 04 742 604.4, Nov 24, 2005; Japan (JP) CNRS Patent 2006-530327, Oct 16, 2006; United States (US) CNRS Patent 018344/0578, Feb 4, 2006.
(9) Reichmann, M. G.; Hollander, F. J.; Bell, A. T. *Acta Crystallogr.* **1987**, *43*, 1681.
(10) (a) Walter-Levy, L.; Férey, G. *Bull. Soc. Chim. Fr.* **1966**, *2*, 482. (b) Walter-Levy, L.; Férey, G. *C. R. Acad. Sci., Ser. C* **1968**, *266*, 99. (c) Golub, A. M.; Tischenko, A. F.; Kikot, I. F. *Russ. J. Appl. Chem.* **1970**, 2159.
(11) O'Keefe, M. A.; Kilaas, R. *MacTempas, V1.70 and Crystalkit V1.77, HRTEM Image Analysis*; Lawrence Berkley National Laboratory: Berkeley, CA, 1987.
(12) *CasaXPS*; Casa Software Ltd.: Teignmouth, U.K., 2005.

$$[Ti_8O_{12}(H_2O)_{24}]Cl_8 \cdot HCl \cdot 7H_2O + (8/R)TMAOH \cdot 5H_2O \rightarrow 8(TiO_2 \cdot nH_2O) + (8/R)(TMACl) + (9 - 8/R)HCl + (27 + 48/R - 8n)H_2O, \quad R > 8/9 \quad (2)$$

The XRD patterns denote the formation of anatase for $0.9 \leq R \leq 1.1$. The diffraction peaks are quite broad (width 1−1.5°) indicating that the coherent length is short, typically less than 10 nm. It is worth noting that drying at 90 °C only also leads to the crystallization of nanocrystalline anatase. Rutile is obtained in more acidic conditions, and for $R = 1.5$, the powder is formed of rods with lengths ranging from 10 to 50 nm (Figures S1 and S2, Supporting Information). The main encountered orientations are [102] and [110], which is the most stable one. Crystallization of such varieties in acidic conditions was already reported.[13] Brookite was also reported to be obtained directly after autoclaving a soluble peroxo−Ti complex in base medium (pH = 10) at 200 °C. The proposed mechanism underlines that the tetrameric Ti cluster may produce in basic medium units that are encountered in brookite structure. More acidic conditions (pH = 6) lead to the crystallization of rutile at 200 °C and anatase at 160 °C. Finally reaction at pH = 3 produces rutile mixed with anatase nanocrystals. No clear relationship could be established between the initial complex and the rutile structure.[14] Below $R = 8/9$, the medium is basic and the reaction can be written as

$$[Ti_8O_{12}(H_2O)_{24}]Cl_8 \cdot HCl \cdot 7H_2O + (8/R)TMAOH \cdot 5H_2O \rightarrow 8[TiO_2 \cdot nH_2O \cdot (1/R - 9/8)TMAOH] + 9TMACl + (36 + 40/R - 8n)H_2O \quad (3)$$

As already mentioned a layered compound is stabilized in very basic conditions and requires to be characterized.

Characterization of the 2D Phase. This lamellar phase is obtained for a R ratio equal or less than 0.47 (8/17), corresponding to the reaction of 17 mol of TMAOH for 1 mol of $[Ti_8O_{12}(H_2O)_{24}]Cl_8 \cdot HCl \cdot 7H_2O$. It is worth noting that for $R = 0.5$ (=8/16), the XRD pattern is very similar to the diagram obtained for $R = 0.6$, indicating that the stoichiometric ratio of the 2D phase is very close to $R = 8/17$.

Thermal Stability. Analysis of the TGA traces performed under air and under Ar when coupled to a mass spectrometer gives some insight of the composition of the layered phase. The experiment is conducted on the solid obtained after drying at 110 °C, that is, including TMACl. In our experimental conditions mass spectrometer information is only reliable when the decomposition takes place under Ar. However, such conditions may induce reductive atmosphere, and the experiment conducted under air is used to propose a formulation. Several weight losses, representing 75% of the initial mass, occur between 25 and 450 °C, where TiO_2 anatase crystallizes (Figure 2a). As evidenced by mass spectrometry (Figure 2b), the first weight loss (I) is only associated with 0.6 water (red line) molecules per Ti atom,

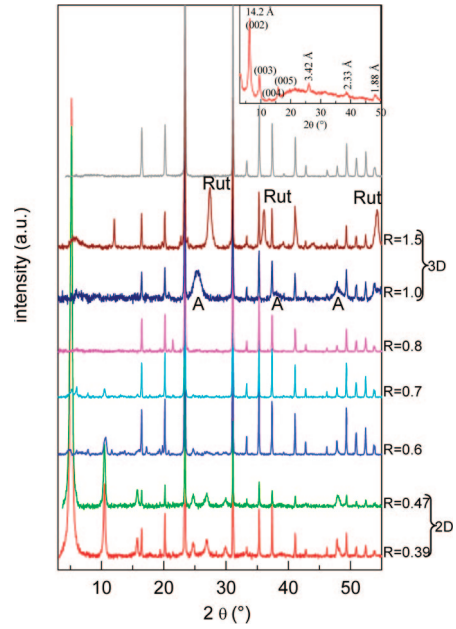

Figure 1. XRD patterns obtained for $1/3 \leq R \leq 3/2$ after solvothermal treatment at 120 °C for 48 h then drying at 110 °C. The diagram of tetramethylammonium chloride (TMACl) (top) is plotted for peak identification. Inset: $R = 0.47$ obtained in ethanol, after drying at 110 °C.

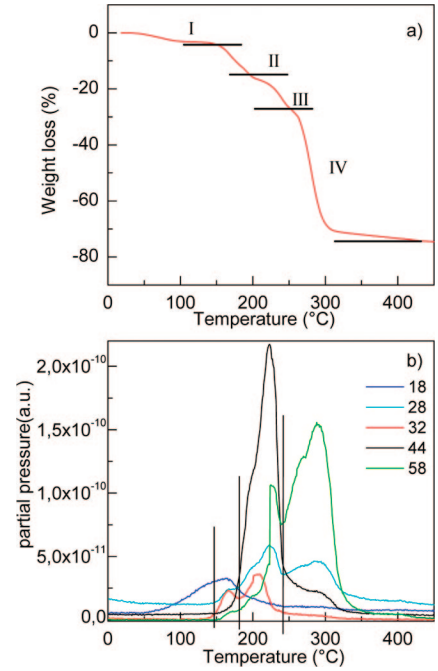

Figure 2. (a) TGA, coupled with (b) mass spectrometry for $R = 0.47$, after drying at 110 °C overnight.

between room temperature and 150 °C. This amount corresponds to 54% of $m/z = 18$ signal indicating that 1.1 water molecules per Ti atoms are present in the solid. The following weight losses between 150 and 450 °C can be divided in three processes: 150−180 °C (II), 180−240 °C (III), and 240−400 °C (IV). The second step is mainly associated with the departure of water ($m/z = 18$), oxygen ($m/z = 16$), and CO ($m/z = 28, 29$), whereas the following step is associated to a strong CO_2 ($m/z = 44$) release, which may correspond either to an oxidation of the TMA^+ cation in presence of water or to the presence of CO_3^{2-} anion due to basic

(13) (a) Potier, A.; Chanéac, C.; Tronc, E.; Mazerolles, L.; Jolivet, J. P. *J. Mater. Chem.* **2001**, *11*, 1116. (b) Potier, A.; Cassaignon, S.; Chanéac, C.; Villain, F.; Tronc, E.; Jolivet, J. P. *J. Mater. Chem.* **2003**, *13*, 877.

(14) Tomita, K.; Petrykin, V.; Kobayashi, M.; Shiro, M.; Yoshimura, M.; Kakihana, M. *Angew. Chem., Int. Ed.* **2006**, *45*, 2378.

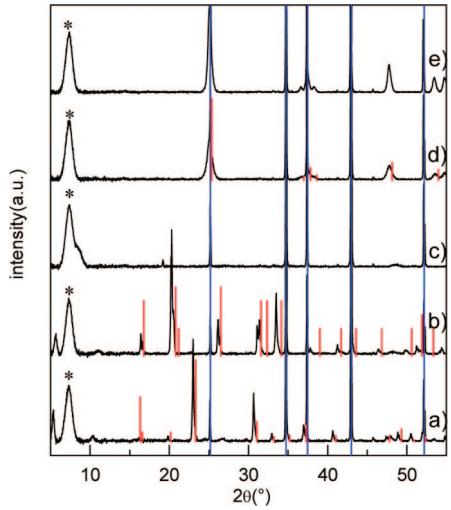

Figure 3. XRD patterns of $R = 0.47$ dried at 110 °C at (a) room temperature, 2D phase and tetragonal TMACl (red bars: JCPDF file no. 21-1922), (b) 175 °C, 2D phase and rhombohedral TMACl (red bars: JCPDF file no. 27-1768), (c) 275 °C, 10.5 Å lamellar phase, (d) 425 °C, anatase (red bars: JCPDF file no. 89-492), and (e) 575 °C, anatase. *, artifact related to the carbon window of the oven; blue bars, alumina of the sample holder.

condition of the process. During the second part of step III fragments belonging to TMA^+ ion are also detected, with the release of $m/z = 58$ which can be attributed to the $(CH_3)_2NCH_2^-$ ion. Smaller amounts of other fragments are also detected, and for clarity they are omitted in Figure 2b. Then between 240 and 400 °C, the decomposition of the TMA^+ cation occurs. The evolution of the XRD pattern with temperature (Figure 3) was recorded to differentiate intermediate steps during this decomposition process and especially to identify the weight loss associated to TMACl. The layered phase (17 Å) is maintained until 175 °C, together with crystallized TMACl. For this compound, as previously described in the literature,[15] a transition from a tetragonal phase (JCPDF file no. 21-1922, Figure 3a) to a rhombohedral one (JCPDF file no. 27−1768, Figure 3b) takes place between 125 and 145 °C. The interlayer distance of the 2D titanium oxo-hydroxide decreases from 17 at 150 °C to 15.7 Å at 225 °C. The coherent stacking is also lost in the process inducing a decrease in the intensities. Then, depending on the heating rate, the rhombohedral form of TMACl may evolve toward the cubic one (JCPDF file no. 27-1767) afterward, this salt decomposes, and its peaks are no more detectable above 275 °C (end of step III). The stacking distance of the layered compound decreases to a lower value of 10.5 Å (Figure 3c) at this temperature. At higher temperatures, the peaks characteristic of this phase disappear, and some broad humps attributed to anatase are distinguishable (Figure 3d,e). This observation allows us to conclude that the degradation of the 10.5 Å layered phase takes place in step IV and that one TMA/Ti is inserted between the layers (based on TGA weight loss). The attribution of steps II and III may also be related to the presence of carbonates in/on the solid due to basic conditions, explaining why a very low amount of TMA^+ fragment is detected. Finally, based on the different weight losses and the initial amount of

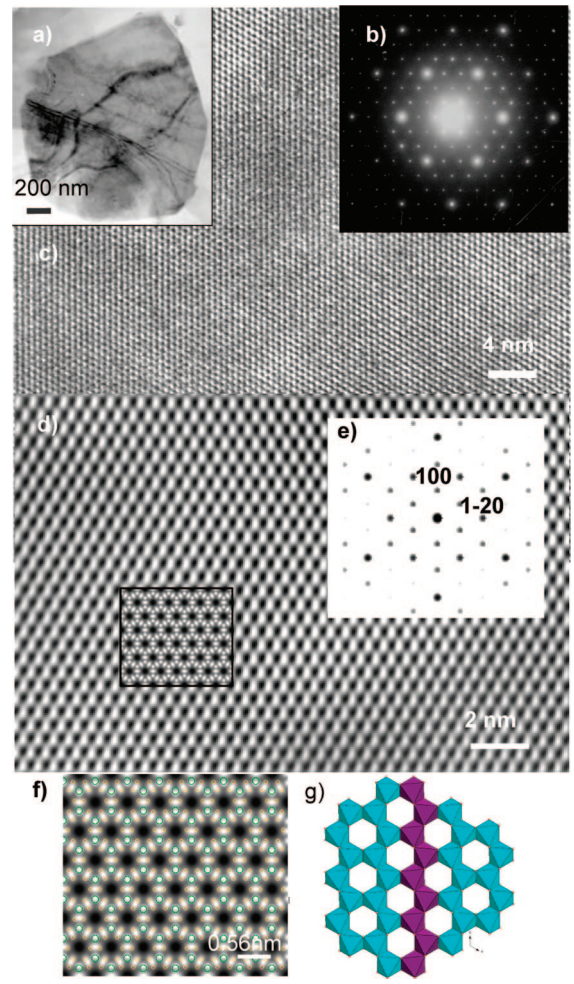

Figure 4. TEM studies of $(TMA)_2Ti_2(O,CO_3)_4(OH)_2$: (a) low-magnification image of the platelet for $R = 0.47$; (b) experimental ED pattern; (c and d) experimental and filtered high-resolution images along [001] showing the hexagonal symmetry with the inset being the calculated image for 60 nm thick foil at −80 nm defocus; (e) calculated ED pattern with (001) zone axis; (f) enlarged and simulated image overlaid with atomic positions; and (g) structural model along [001].

reactant, the solid would be written $(TMA)_2Ti_2O_{3.30}(CO_3)_{0.70}(OH)_2 \cdot 1.22H_2O$, (9/4)TMACl.

Crystallographic Study. To compliment the XRD experiments which suggest for the $R = 0.47$ phase a two-dimensional (2D) structure with an interlayer *d*-spacing of 17 Å, the (110) perpendicular plane was investigated by TEM. Figure 4 shows some electron micrographs of this lamellar phase. The low-magnification image (Figure 4a) clearly demonstrates that the $R = 0.47$ compound exhibits a platelet morphology with a quasi regular shape and diameter of 1.5 μm. The electron diffraction (ED) pattern and experimental high-resolution images (Figure 4b,c) reveal the hexagonal symmetry of the 2D titanate. The experimental image was processed to improve the observed contrasts, and the filtered image is depicted in Figure 4d with the simulated high-resolution TEM (HRTEM; inset of Figure 4d) and ED images (Figure 4e). The 2D structure consists of thin layers with a periodicity of 5.6 Å, deduced from the distance between the parallel dark dots on the filtered image. Among the numerous titanates with lamellar structures and hexagonal symmetry, only the mineral $CaTi_2O_4(OH)_2$ (kassite)[16] can be retained with respect to the TEM and XRD results. The

(15) Dufourcq, J.; Haget-Bouillaud, Y.; Chanh, N.; Lemanceau, B. *Acta Crystallgr., Sect. B* **1972**, *28*, 1305.

kassite framework is a common structure type for oxides, hydroxides, and fluorides, with general composition AM_2X_6. It is based on a distorted hexagonal-close-packing of anions, with alternate (001) layers of octahedral sites that are two-thirds occupied by M atoms and one-third occupied by A atoms. The MX_6 octahedra share edges in a honeycomb arrangement (Figure 4g) as in gibbsite or corundum, giving a layer composition $[M_2X_6]^{n-}$. The A atoms sit above and below the empty octahedral sites in the M_2X_6 layers, resulting in the AO_6 octahedra corner-sharing with three MX_6 octahedra from the hexagonal rings on either side (see Figure S3, Supporting Information). On the basis of these considerations, we thus propose that the lamellar phase presents an structure analogous to that of kassite, with the formulation $(TMA)_2Ti_2O_4(OH)_2 \cdot nH_2O$, where the anionic layer is compensated by two TMA^+ cations instead of one Ca^{2+} in the octahedral environment. Compared to the kassite structure, the interlayer spacing reaches 17 Å instead of 4.68 Å when Ca^{2+} lies in the gallery. According to the clathrate structure of $TMAOH \cdot 5H_2O$,[17] the distance between two contiguous TMA^+ ions surrounded by water molecules can be estimated to be 13.5 Å. Most likely, the proposed structural model for $(TMA)_2Ti_2O_4(OH)_2 \cdot nH_2O$ consists of a layered arrangement of distorted $[Ti_2O_4(OH)_2]^{2-}$ units sharing edges, and in between each TMA^+ layer is separated by interlayer water molecules. This conclusion is further supported by the fact that an anhydrous form with interlayer spacing equal to 14.5 Å can be isolated when the reaction is performed in ethanol instead of water. Using a kassite-like structure in projection along [001], the observed contrasts on the filtered image fit quite well with that calculated for a defocus value of −80 nm and a lamellar thickness equal to 60 nm (Figure 4f). The lack of contrast along the [100] direction results from a 1.8 Å periodicity of Ti−O atomic columns, which is close to the resolution limit. The calculated ED pattern (Figure 4e) in projection along [001] is also in reasonable agreement with the experimental ED pattern (Figure 4b).

The powder obtained by annealing at 575 °C for 2 h in air exhibits an XRD pattern characteristic of anatase (Figure 5). The rather broad peaks are related to the size of the platelet-like crystals of 20 nm diameter as found by TEM (Figure 5, inset). A close examination of several crystallites allows us to conclude that the most encountered orientation is the [101] zone axis of anatase. The comparison of the XRD patterns obtained in a capillary (ramdomly oriented sample) and in Bragg−Brentano geometry (Figure 5) also confirms this preferential orientation.

Effect of Rinsing with Distilled Water for $0.47 \leq R \leq 0.8$. To eliminate TMACl, the solids obtained after autoclaving at 120 °C and drying at 110 °C were rinsed three times with 50 mL of water for 10 min each and dried in air at 110 °C.

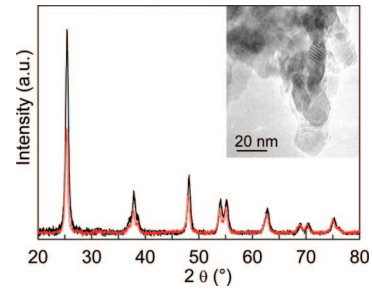

Figure 5. XRD pattern of anatase obtained by heating $R = 0.47$, at 550 °C for 2 h under air. Red, randomly oriented sample set in a capillary; black, Bragg−Brentano geometry, inducing a preferential orientation due to the morphology of the platelets. Inset: TEM image of anatase obtained by annealing of $R = 0.47$ for 2 h at 550 °C.

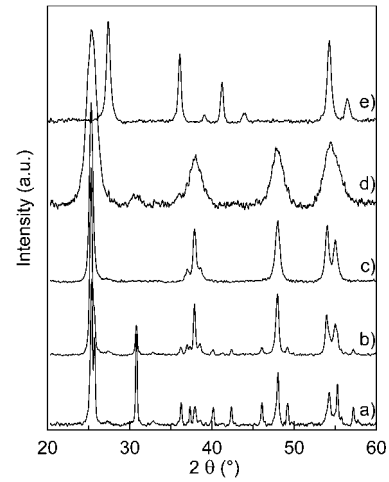

Figure 6. XRD patterns of different samples rinsed with water and dried at 110 °C: (a) $R = 0.6$, brookite; (b) $R = 0.7$, brookite and anatase; (c) $R = 0.8$, anatase; (d) $R = 1$, anatase and brookite; and (e) $R = 1.5$, rutile.

Table 1. Cell Parameters and Density of LT-Brookite ($R = 0.6$, Rinsed), Brookite, LT-Anatase ($R = 0.8$, Rinsed), and Anatase

	LT-brookite	brookite[19]	LT-anatase	anatase[20]
a (Å)	9.180(3)	9.174(2)	3.786(1)	3.7840(7)
b (Å)	5.454(1)	5.449(2)		
c (Å)	5.140(1)	5.138(2)	9.481(3)	9.500(2)
V (Å^3)	257.37(1)	256.84	135.90(3)	136.03
density	4.00(1)	4.14	3.67(1)	3.90

Chemical Characterization. No obvious change was observed for the samples obtained in the condition $R \geq 0.9$, except the expected disappearance of TMACl. However, for the intermediate R values this process enables the crystallization of brookite for $0.47 \leq R \leq 0.6$, anatase for $R = 0.8$, and a mixture of both polytypes for $R = 0.7$ (Figure 6). The sharpening of the diffraction peaks suggests that the crystallite sizes are larger than in the particles obtained in more acidic conditions. In the following, the brookite obtained for $R = 0.6$ is denoted LT-brookite, and the anatase starting from $R = 0.8$ is denoted LT-anatase. The cell parameters are refined using FULLPROF.[18] The results are gathered in Table 1. The cell parameters are not significantly different

(16) (a) Kukharenko, A. A.; Orlova, M. P.; Bulakh, A. G.; Bagdasarov, E. A.; Rimskaya-Korsakova, O. M.; Nefedov, Y. I.; Ilyinskiy, G. A.; Sergeyev, A. C.; Abakumova, N. B. *The Caledonian complex of ultrabasic alkalic rocks and carbonatites of the kola peninsula and northem karelia*; Nedra: Moscow, 1965; p 368. (b) Self, P. G.; Buseck, P. R. *Am. Mineral.* **1991**, *76*, 283. (c) Grey, L. E.; Mumme, W. G.; Pekov, I. V.; Pushcharovsky, D. Y. *Am. Mineral.* **2003**, *88*, 1331.

(17) Hesse, W.; Jansen, M. *Z. Anorg. Allg. Chem.* **1991**, *595*, 115.

(18) Rodriguez-Carvajal, J. *FULLPROF: A program for Rietveld Refinement and Pattern Matching Analysis*; Abstracts of the satellite meeting on powder diffraction of the XVth Congress of the IUCr, Toulouse, France, 1990; p 127; *J. Physica B.* **1993**, *192*, 55.

from those of bulk brookite[19] or anatase.[20] However, the densities are significantly smaller than expected for both varieties (Table 1): 4.00(1) for 4.14 for LT-brookite and bulk brookite and 3.67(1) for 3.90 for LT-anatase and bulk anatase, respectively.

IR spectra (inset Figure 7a) indicate the presence of water molecules[21] through a deformation vibration located at 1628 and 1631 cm^{-1} for LT-brookite and LT-anatase, respectively. In addition, stretching vibrations of O−H are detected with two broad peaks at 3480 and 3300 cm^{-1} in LT-brookite and a large hump at 3430 cm^{-1} for LT-anatase. In this region lie characteristic wavenumbers of stretching vibrations of TiO_2 surface hydroxyl groups and adsorbed water molecules.[21] Moreover, carbonate stretching vibrations appear at 1561 and 1484 cm^{-1} and 1561 and 1484 cm^{-1} for LT-brookite and LT-anatase, respectively. These vibrations lie in the range of ν_3, the asymmetric stretching vibrations of ionic carbonate and their split positions when coordination to a metal cation is observed.[22] The incorporation of carbonate species may be related to basic conditions in the initial suspension and to the stability of the CO_3^{2-} anion in solution. Before autoclaving the pH values are 12.8 and 8 for $R = 0.6$ and $R = 0.8$, respectively, whereas after reaction the suspension is more basic with pH = 13.9 and 13.5 for both ratios.

TGA experiments performed under argon and coupled with a mass spectrometer allow us to confirm the existence of water or hydroxides and carbonates on the solids (Figure 7). The water ($m/z = 18$) departure takes place between 200 and 800 °C for LT-brookite and up to 1100 °C for LT-anatase. It is also associated to different CO releases: a continuous departure from room temperature to 200 °C, followed by two peaks at 350 and 480, for both compounds, and then the last two at 860 and 1050 °C for LT-brookite and 930 °C for LT-anatase. These differences in release temperatures are probably related to different binding energies. The first weight loss is attributable to CO_2 coming from carbonates adsorbed on the surface because they are released before 200 °C.

XPS analysis (Table 2) also proves that carbonate anions[23] could be detected in both samples through the characteristic peaks at 288.5 and 288.1 eV (C_b) in addition to the peak attributable to pollution (C_p, calibrated to 284.7 eV) and the intermediate peak at 286.2 eV (C_a) which can be assigned to carbon connected to nitrogen atoms[24] coming from residual tetramethyammonium and trimethylamine. The latter may result from a breaking of one $-N-CH_3$ bond in part of the tetramethylammonium cations. Traces of Cl^- could also be detected. We did not consider them in the following because they represent less than 1 atom % in the solid. The

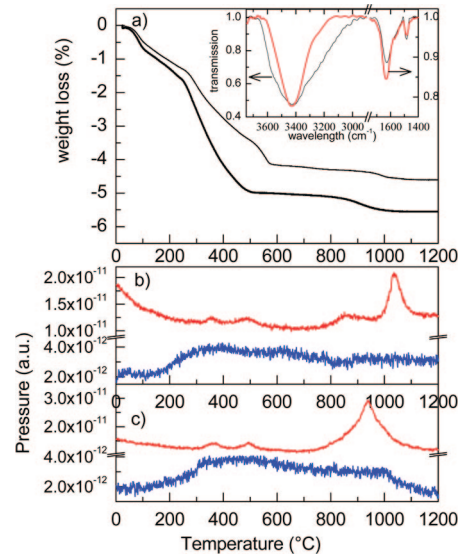

Figure 7. (a) TGA traces, for LT-brookite (thin line) and LT-anatase (thick line) obtained from $R = 0.6$ and $R = 0.8$, after drying, washing, and second drying at 110 °C. Inset: IR spectra LT-brookite (black) and LT-anatase (red). Mass spectrometry results: red, $m/z = 28$, and blue, $m/z = 18$, for (b) LT-brookite and (c) LT-anatase.

Table 2. Decomposition of Core Level XPS Peaks for LT-Brookite and LT-Anatase

	position (eV)	$R = 0.6$ fwhm (eV)	atom %	position (eV)	$R = 0.8$ fwhm (eV)	atom %
O_a	529.7	1.20	57.6	529.4	1.20	54.4
O_b	531.2	2.08	12.2	530.8	2.35	16.5
Ti $2p_{3/2}$	458.4	1.11	27.3	458.2	1.12	26.1
C_b	288.5	1.63	2.8	288.1	1.60	3.0

N and Cl detected but lower than 1 atom %

O 1s peak at lower binding energy (O_a, close to 530 eV) is assigned to the oxygen anion belonging to the Ti−O framework[25] whereas the other peak (O_b, close to 531 eV) at higher binding energy is characteristic of oxygen atoms belonging to carbonate through an O=C bond.[23] The excess of oxygen atoms with respect to C_b confirms that hydroxide or water molecules are present in the materials, because such species also appear at a position close to 531 eV.[26] The estimated amounts of carbonate and water molecule contents are close to 0.10 and 0.13, respectively, per Ti atom for LT-brookite and to 0.12 and 0.28, respectively, per Ti atom for LT-anatase. From this chemical analysis we cannot distinguish the amount of hydroxide from the water molecule. The following formulas could then be determined for the two compounds: $TiO_{1.83+w/2}(CO_3)_{0.10}(OH)_{0.13-w}(H_2O)_w$, $0 < w < 0.13$, and $TiO_{1.74+w/2}(CO_3)_{0.12}(OH)_{0.28-w}(H_2O)_w$, $0 < w < 0.28$ for LT-brookite and LT-anatase, respectively. The carbonate amount is an upper limit because we probably overestimated the proportion. This might be the case, in particular, for carbonates adsorbed on the surface which are released before 200 °C. To correlate this quantification with TGA analysis, we estimated that the carbonate amount lies between 0.06 and 0.03 (depending on w) in LT-brookite and reaches 0.05

(19) Meagher, E. P.; Lager, G. A. *Can. Mineral.* **1979**, *17*, 77.
(20) Ballirano, P.; Caminiti, R. *J. Appl. Crystallogr.* **2001**, *34*, 757.
(21) Bezrodna, T.; Puchkovska, G.; Shimanovska, V.; Chashechnikova, I.; Khalyavka, T.; Baran, J. *Appl. Surf. Sci.* **2003**, *214*, 222–231.
(22) Nakamoto, K. *Infrared and Raman Spectra of Inorganic and Coordination Compounds*, 4th ed.; Wiley: New York, 1986; pp 123−124.
(23) Bhaskar, S.; Allgeyer, D.; Smythe, J. A. III *Appl. Phys. Lett.* **2006**, *89*, 254103.
(24) Briggs, D.; Grant, J. T. *Surface analysis by Auger and X-ray photoelectron Spectroscopy*; IM publication: Chichester, 2003.
(25) Moulder, J. F.; Stickle, W. F.; Sobol, P. E.; Bomben, K. D. *Handbook of X-ray Photoelectron Spectroscopy*; Perkin-Elmer Corp.: Eden-Prairie, 1992.
(26) (a) Yu, J. C.; Zhang, L.-Z.; Zheng, Z.; Zhao, J. C. *Chem. Mater.* **2003**, *15* (11), 2280. (b) Gao, Y.-F.; Masuda, Y.; Koumoto, K. *Langmuir* **2004**, *20*, 3188.

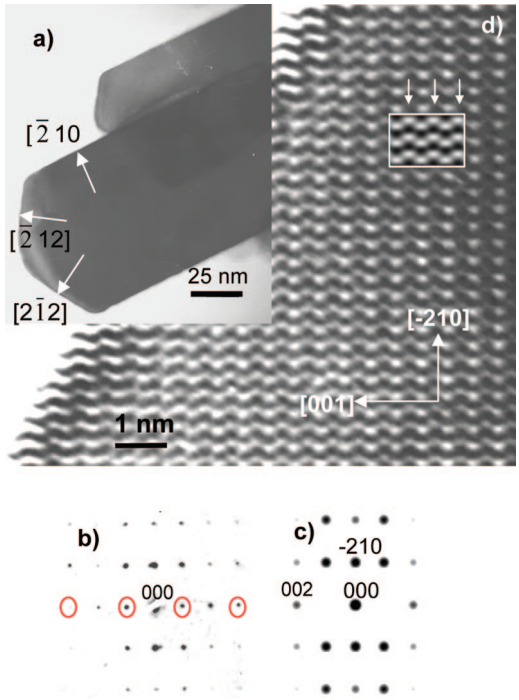

Figure 8. TEM studies of LT-brookite ($R = 0.6$): (a) low-magnification image of the stick; (b) experimental ED pattern; (c) calculated ED pattern with standard brookite structure, along the [120] zone axis; and (d) experimental high-resolution images along [120] showing the orthorhombic symmetry; the inset image is calculated for 3 nm thick foil at −40 nm defocus (white arrows indicate the supercell periodicity along [001]).

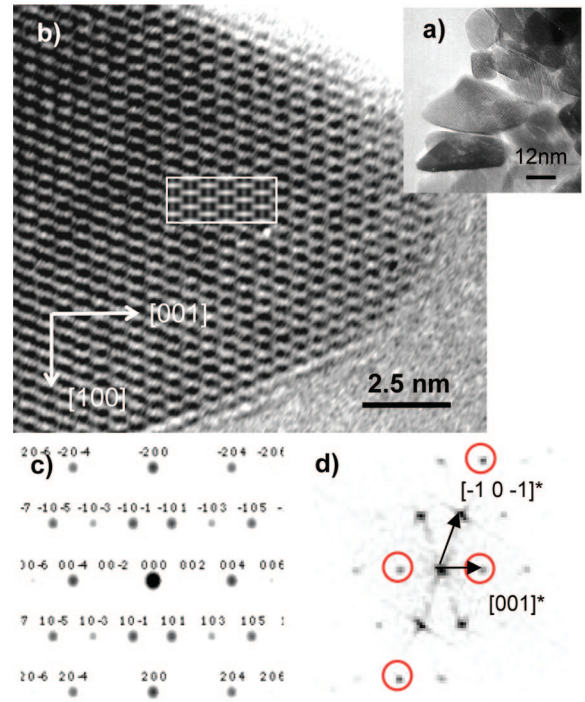

Figure 9. TEM studies of TiO_2 LT-anatase ($R = 0.8$) after washing and drying at 110 °C; (a) low magnification TEM image; (b) experimental high resolution TEM image along [010], the inset calculated image is for 3 nm thick foil at −30 nm defocus; (c) simulated ED pattern along the [010]; (d) FT of HRTEM image along [010] zone axis exhibiting extra spots, surrounded by red circles.

at the most ($w = 0$) per Ti^{4+} cation for LT-anatase. We infer that the presence of adsorbed species on the nanoparticles induces an overestimated volume during the density measurements. A rough calculation accounting for the molecular volume occupied by CO_2 or water molecules (in the solid state) is coherent with this hypothesis (Supporting Information).

TEM Study. The low magnification image of as-prepared LT-brookite (Figure 8a) shows well-facetted crystals with growth direction along the [001] axis. Typically, the ($\bar{2}$10) and (120) planes are found in brookite powdered materials, together with some ($\bar{2}$12)/(2$\bar{1}$2). For all samples numerous long sticks are observed that are several hundred nanometers in length and approximately 30−80 nm in width. The selected area electron diffraction (SAED) of LT-brookite along [120] (Figure 8b) gives evidence for two main characteristic distances of 0.35 and 0.52 nm with no special reflection conditions. These observations are not in agreement with the *Pbca* space group extinctions previously reported for the brookite structure[19] and particularly for the reflection condition (00*l*): $l = 2n$. In comparison with the ED pattern shown in Figure 8c, few supplementary peaks (marked by red circles) appear along the [001]* direction. The persistence of these satellite spots by tilting the crystal with respect to the incident electron beam excludes the double diffraction phenomenon. A reinforcement of the intensity every two white dots along [001] can also be seen on the experimental HRTEM image (see white arrows) which is not evidenced on the calculated image (inset Figure 8d) based on the conventional structure data of brookite.

The LT-anatase (obtained from $R = 0.8$ and rinsing) crystallizes as smaller objects in the range of 10−40 nm. These values are quite coherent with the widening of diffraction peaks. A rough evaluation of the coherent crystalline length using the Scherrer formula leads to a value close to 20 nm, indicating that the particles are single crystals. LT-anatase nanocrystallites typically expose the (101) and (100)/(010) crystal faces (Figure 9a) together with some (001). An accurate analysis of the HRTEM and ED diffraction patterns along both directions reveals significant differences with those of standard anatase crystallites. The HRTEM image (Figure 9b), showing well-facetted crystals with growth direction along [001] axis, is quite well simulated using anatase data with 3 nm thick foil at −30 nm defocus. But the comparison of simulated ED pattern (Figure 9c) and Fourier transform (FT; Figure 9d) along the [001] zone reveals that supplementary peaks, marked by red circles, appear along [00l]* and [101]* directions. In comparison to the calculated ED pattern for anatase (Figure 10b), the FT (Figure 10c) of the LT-anatase experimental HRTEM image (Figure 10a) with [111] zone axis also exhibits numerous extra spots (surrounded by red circles), both along the [*hh*0]* and [*hh*2*l*]* directions involving a doubling of cell parameters. Assuming that these satellite peaks do not originate from double diffraction phenomena, the LT-anatase structure slightly differs from the conventional anatase. The latter is known to crystallize in tetragonal symmetry, $I4_1/amd$ space group, with the special reflection conditions: *hkl* with $h + k + l = 2n$; *hk*0, $h, k = 2n$; *hhl*, $2h + l = 4n$; 0*kl*, $k + l = 2n$; and 00*l*, $l = 4n$. The HRTEM

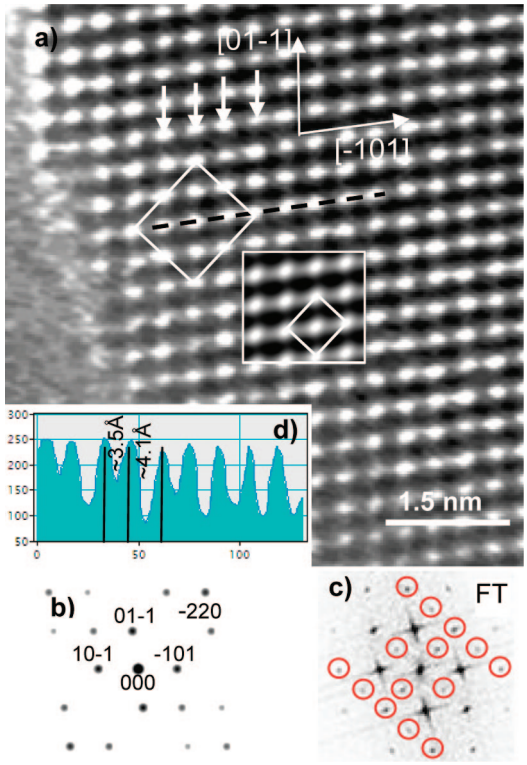

Figure 10. TEM studies of TiO_2 LT-anatase ($R = 0.8$) after washing and drying at 110 °C; (a) experimental high resolution TEM image along [111], the inset calculated image is for 3 nm thick foil at −40 nm defocus (white arrows indicate the supercell periodicity along $[\bar{1}01]$); (b) simulated ED pattern along the [111]; (c) FT of HRTEM image along [111] zone axis exhibiting numerous extra spots, surrounded by red circles; and (d) histogram of the intensities along $[\bar{1}01]$ (black dashed line).

image (Figure 10a) analysis reveals that the existence of a supercell results from a local distortion. According to the anatase structure, the simulated HRTEM image along [111] for 3 nm thick foil at −40 nm defocus (inset Figure 10a) highlights a regular centered cell with two main characteristic distances at 0.38 nm along the $[\bar{1}01]$ and $[01\bar{1}]$ directions. The experimental HRTEM image (Figure 10a) shows regular white contrasts with successive short (S) and long (L) distances along $[\bar{1}01]$ indicated by the white arrows. A histogram performed along this direction (Figure 10d) clearly demonstrates the succession of $S = 0.35$ nm and $L = 0.41$ nm spacing involving a periodicity doubling along $[\bar{1}01]$. Consequently, the distortion magnitude of the framework can be estimated to 0.025 nm along $[\bar{1}01]$ with respect to the conventional anatase structure. Furthermore, the S and L distances along $[\bar{1}01]$ are stacked with antiphase arrangement along $[01\bar{1}]$, and the deduced LT-anatase supercell is four times larger than the anatase one, as indicated in Figure 10a. Despite these modifications that clearly appear on the HRTEM images, their amplitude is too weak to induce any superstructure on the XRD pattern. Therefore, the average cell parameters are quite similar to those of anatase (Table 1), in a first approximation.

The present TEM study clearly evidences a periodic distortion of the Ti−O framework in LT-brookite and LT-anatase nanocrystallites which could originate from chemically bonded species such as HCO_3^- or CO_3^{2-} water or hydroxyl groups. As a result of the small thickness of the

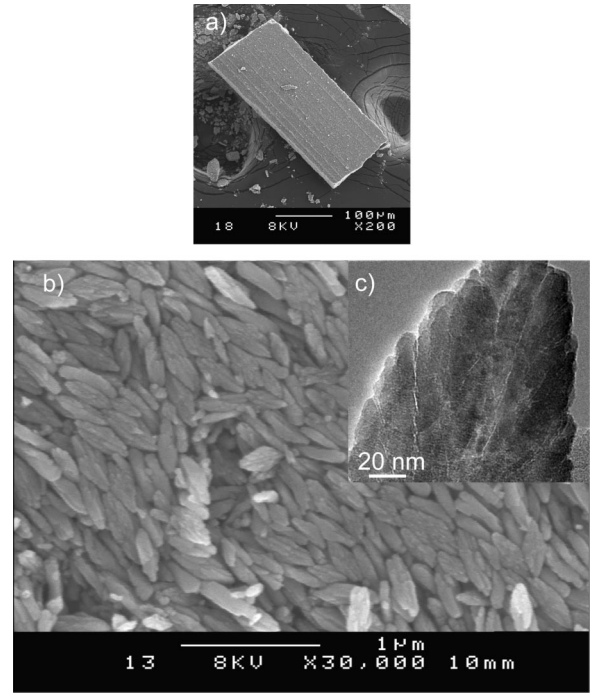

Figure 11. SEM images of (a) organizations of brookite from $R = 0.47$ obtained after rinsing with water and drying at 70 °C (130 × 300 μm^2), (b) zoom of the surface evidencing the size of the particles (length, 200−400 nm; width, 50 nm), and (c) TEM image.

nanocrystals (3 nm), the surface stress resulting from the adsorbed species induces a structural modulation which is propagated into the bulk. Such species might belong to the Ti−O surface through, for instance, μ_2-oxygen atoms on the (101), (100), or (001) surface planes. On the basis of crystallographic data and the average surface of nanocrystallites, the amount of these available sites can be estimated to be 0.04/Ti. This conclusion is corroborated by the TGA/MS, XPS analysis, and density measurements.

Reactivity and Shaping. The aqueous chemical growth process mentioned above is developed to produce thin films and coatings of titanium oxide materials onto various substrates at low cost and low temperature. Such a method allows the preparation of advanced nano-, meso-, and microparticulate thin films as well as two- and three-dimensional arrays, without any template, surfactant, or external field and without any specific requirements in substrate activation, thermal stability, or crystallinity.[27,28] In our case, the high reactivity of these powders leads to an organization of the particles of brookite starting from $R = 0.47$ and LT-anatase starting from $R = 0.8$ preparation. After autoclaving, the suspension is dried in an oven at 110 °C. After rinsing and another drying at 70 °C for $R = 0.47$ and 110 °C for $R = 0.8$, the nanoparticles self-arrange as parallelepipeds with dimensions in the micrometer range. For brookite, the particles are elongated as rice grains and roughly arranged along the large axis, leading to parallelepipeds as shown in Figure 11a. These platelets exhibit a brittle contrast when observed using binoculars. The SEM image allows us to evidence that the size of the particles forming the platelets

(27) Vayssieres, L. *C. R. Chim.* **2006**, *9*, 691.
(28) Vayssieres, L. *Appl. Phys. A: Mater. Sci. Process.* **2007**, *89*, 1.

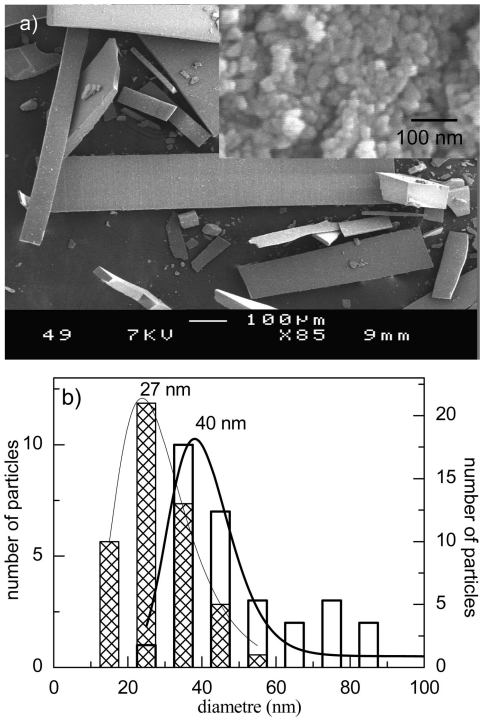

Figure 12. (a) SEM image of organizations of LT-anatase obtained after rinsing with water and drying at 110 °C of $R = 0.8$. Inset: zoom of the surface evidencing the size of the nanoparticles (30−50 nm) in agreement with TEM images (Figure 8a), (b) size distribution of particles fitted to a log-normal distribution centered on 27 nm for LT-anatase (hatched) and 40 nm (empty) with malonic acid.

is length, 200−400 nm, and width, 50 nm (Figure 11b). Moreover, TEM higher magnification images indicate that the latter platelets are formed of smaller nano-objects (Figure 11c). $R = 0.8$ LT-anatase particles also arrange as platelets with the following typical dimensions: 10−960 μm long, 30−180 μm large, and 10−40 μm thick (Figure 12a). As shown in the inset enlarged image of the surface, the particle size is around 27 nm. Adding a complexing agent such as malonic acid enables the size of the nanoparticles to be tuned to 40 nm (Figure 12b), and their aggregation process is also modified. In this condition, the arrangement of the nanoparticles produces larger platelets: >1 mm long, 500 μm wide, and 10−40 μm thick, which in both cases are also brittle.

Discussion

The presence of a 2D phase during the hydrolysis of Ti alkoxide by TMAOH has already been observed by Chemseddine and Moritz.[6] This intermediate was observed when Ti/TMAOH = 0.84 is treated under reflux for 6 h with a far smaller titanium concentration (7×10^{-6} mol·L^{-1} instead of 6×10^{-1} mol·L^{-1} here). Nanocrystals (13.5 nm in dimension) hexagonally self-assemble as a superlattice leading to 0.3−1 μm arrangement. Their interpretation was related to the formation of TMA^+/Ti clusters inside the nanocrystals exhibiting a layered structure with a stacking periodicity of 16.5 Å. The extension of the slabs could be related to the difference in titanium concentration and low temperature synthesis under reflux. Titanium alkoxides ($Ti(OR)_4$) which are dissolved in an alcohol and hydrolyzed by the addition of water under acidic, neutral, or basic conditions are highly moisture sensitive. The rapid hydrolysis rate of $Ti(OEt)_4$ ($k_h = 10^{-3}$ mol^{-1} L s^{-1}) induces gelation times of the order of seconds or minutes, and thus the nucleation and growth are never separated into two steps. Using the $[Ti_8O_{12}(H_2O)_{24}]Cl_8 \cdot HCl \cdot 7H_2O$ cluster allows us to control the condensation of the Ti−O framework starting with a more concentrated suspension than when alkoxides are involved. The first step involves dissolution of the cluster crystals, construction of the framework takes places in a second step, and finally drying at low temperature in the presence of TMA^+ cations leads to the 2D arrangement. A layered phase with a stacking parameter close to 17 Å was also reported when layered pseudolepidocrocite titanates are exfoliated leading to a colloidal solution[29] in presence of tetrabutylammonium hydroxide. Here, it must be noted that the 2D structuration takes place during drying at 110 °C in presence of TMACl and TMAOH. The solid and liquid parts could be separated by centrifugation. Upon evaporation of water from the supernatant, the 2D phase crystallizes after drying at 110 °C. The presence of tetramethylammonium salts is required to obtain the bidimensional arrangement, due to the structuring property of tetramethylammonium cations. This observation explains why for $8/17 < R < 8/9$, after drying, the characteristic peaks in the XRD pattern of the 2D phase are not discernible since the amount of TMAOH is not sufficient. Washing the 2D compound obtained in basic conditions (pH = 12.8 before autoclave) induces the formation of brookite ($R \leq 0.6$) by condensation of the layers. When the amount of TMAOH is lower (pH = 8 before autoclaving), condensation toward anatase ($R = 0.8$) takes place. Before drying the XRD pattern is already characteristic of brookite and anatase for $R = 0.6$ and $R = 0.8$, respectively. As already reported, pH seems to be a crucial parameter for the selective synthesis of titania polytypes, but recent works also tend to indicate that the nature of counterions is also determinant.[30] Here, washing with distilled water, the solid obtained in the basic medium, removes the TMACl salt and TMA^+ cations necessary to the stabilization of the 2D structure. Therefore, addition of water induces a relative acidification of the medium which promotes the condensation toward brookite and anatase. It is interesting to note that a zigzag chain (purple in Figure 4) formed by octahedra sharing edges is a common feature in the layered compound $(TMA)_2Ti_2O_4(OH)_2 \cdot nH_2O$ and brookite or anatase (Figure S4, Supporting Information). In both varieties these chains are connected by edge sharing in different manners. A partial dissolution of the 2D structure and topotactic condensation of these chains cannot be excluded to account for the 2D to 3D phase transformation. Unfortunately, such a topotatic mechanism is difficult to prove experimentally but both anatase and brookite nanocrystallites exhibit preferential orientations. An adsorption of a small amount of carbonate and water molecules or

(29) (a) Sasaki, T.; Watanabe, M.; Hashizume, H.; Yamada, H.; Nakazawa, H. *J. Chem. Soc., Chem. Commun.* **1996**, 229. (b) Sasaki, T.; Watanabe, M.; Hashizume, H.; Yamada, H.; Nakazawa, H. *J. Am. Chem. Soc.* **1996**, *118*, 8325. (c) Sasaki, T.; Watanabe, M. *J. Phys. Chem. B* **1997**, *101*, 10159.
(30) Cassaignon, S.; Koelsch, M.; Jolivet, J.-P. *J. Mater. Sci.* **2007**, *42*, 6689.

hydroxide on the anionic framework is noticed and accounts for the low experimental density values and the superstructures observed in HRTEM images on these samples.

Conclusion

The low-temperature aqueous chemical growth enables the control of the size of TiO_2 nano-, meso-, and microcrystallites and their surface morphology, as well as their crystal structure. Under autogenous conditions, at 120 °C, the hydrolysis of an original precursor of Ti oxide, $[Ti_8O_{12}(H_2O)_{24}]Cl_8 \cdot HCl \cdot 7H_2O$, by TMAOH hydroxide leads to the formation of a 2D phase for R = Ti/TMAOH < 8/17, whereas 3D frameworks are obtained in more acidic conditions, for R > 8/9, anatase and then rutile. For 8/17 < R < 8/9, the solids are amorphous by XRD, but after rinsing with water and drying at 110 °C, brookite or anatase can be obtained as nanocrystalline powders. These low temperature oxides containing hydroxide and carbonate species exhibit a modulated structure evidenced by TEM studies. TGA/MS, XPS, and experimental densities agree with a small amount of adsorbed species estimated (per Ti atom) to 0.06 carbonate and 0.13 water or hydroxide for LT-brookite and 0.05 carbonate and 0.28 water or hydroxide for LT-anatase. We also demonstrate that starting from the 2D phase brookite is obtained at a temperature as low as 70 °C. This novel and inexpensive bottom-up approach is developed to produce thin films and coatings of titanium oxide with controlled allotropic variety (brookite, anatase, or rutile) and crystallite orientation onto various substrates and at low temperature. The monodispersed titanium oxide nanoparticles can be stabilized in colloidal solutions and then coated by sedimentation, solvent evaporation, or spin and dip-coating processes to form nanostructured thin films.

Acknowledgment. The authors thank E. Gautron for TEM, A. Barreau for SEM, S. Grolleau for TGA/MS, P.-E. Petit for XRD, J. Hamon and V. Fernandez for XPS, and M. Kurmoo. C.-E.L. is indebted to the ANR-PV for financial support.

Supporting Information Available: Figures S1−S3, comment on carbonate adsorption, and Figure S4 (PDF). This information is available free of charge via the Internet at http: //pubs.acs.org.

CM800716F